Update on Validation and Incorporation of a New Steel Corrosion Module into Fuel Matrix Degradation Model

Spent Fuel and Waste Disposition

Prepared for
US Department of Energy
Spent Fuel and Waste Science and Technology

James Jerden
Vineeth Kumar Gattu
William Ebert
Argonne National Laboratory

M4SF-18AN010301017
M4SF-18AN010302016
August 6, 2018

This work was supported by the US Department of Energy, Office of Nuclear Energy. The report was prepared at Argonne National Laboratory as part of the Spent Fuel and Waste Science and Technology Campaign.

SUMMARY

This work is being performed as part of the DOE NE Spent Fuel and Waste Science and Technology Campaign Argillite and Crystalline Rock R&D work packages: SF-18AN01030101 and SF-18AN01030201. This document meets the milestone M4SF-18AN010301017 for Argillite R&D and the milestone M4SF-18AN010302016 for Crystalline R&D.

This report updates work reported in Jerden et al., 2017(a) and Jerden et al., 2017(b) that discuss the incorporation of a steel corrosion module as the primary source of H_2 into the fuel matrix degradation (FMD) model.

The FMD model is being developed to predict radionuclide source term values based on fundamental electrochemistry and thermodynamics that calculates the degradation rate of spent UO_2 fuel. The FMD model has been implemented in a manner that facilitates its integration with the generic disposal system analysis (GDSA) performance assessment (PA) model and a preliminary integrated FMD-GDSA model has been successfully tested (Jerden et al., 2017(b)). The specific focus of on-going work is to accurately and quantitatively represent the generation of H_2 in a breached waste package and model its effect on the degradation rate of the spent fuel so that this key process can be accurately represented in PA models.

It has been shown experimentally that millimolar concentrations of dissolved H_2 in contact with spent fuel will inhibit oxidative dissolution thus decreasing the fuel degradation rates by 3 – 4 orders of magnitude (e.g., Röllin et al., 2001, Ollila, 2008). This will lead to a significant decrease in the radionuclide source terms used in repository PA models. A recent sensitivity study showed the dissolved H_2 concentration is the dominant environmental variable affecting the UO_2 spent fuel dissolution rate (Jerden et al., 2015). Therefore, on-going experimental and modeling efforts addressing this process are a high priority.

The anoxic corrosion of metallic engineering materials will be the main source of H_2 in crystalline and argillite rock repository systems, including stainless steel and carbon steel internal waste package components and possibly the Zircaloy fuel cladding. A steel corrosion module has been added to the FMD model to account for these H_2 sources and couple the H_2 generation rate with fuel degradation processes. As discussed below, there is a need for experimental data from electrochemical corrosion experiments with relevant steel, Zircaloy and UO_2 electrodes to parameterize and validate the steel corrosion module in the FMD model with regard to key environmental variables and alloy compositions.

Based on comparisons of model results and existing data, it was concluded that new experimental work is needed to provide electrochemically determined corrosion rates for relevant engineering materials (steels, Zircaloy) under conditions relevant to crystalline and argillite rock disposal environments. This report presents results from the updated FMD model (FMDM V.4) and summarizes the electrochemical experimental work being performed to parameterize and validate the FMDM steel corrosion module. The updates discussed below were made to parameter values for key redox reactions based on existing experimental data.

This page is intentionally left blank.

This page is intentionally left blank.

LIST OF FIGURES

LIST OF TABLES

ACRONYMS

CMPM	Canadian Mixed Potential Model
DOE	U.S. Department of Energy
FEPs	Features, events, and processes
FMD	Fuel matrix degradation (model)
FMDM	Fuel matrix degradation model
GDSA	Generic Disposal System Analyses
ICP-MS	Inductively coupled plasma-mass spectrometry
MCNPX	Monte Carlo N-Particle eXtended
ORNL	Oak Ridge National Laboratory
PA	Performance assessment
R&D	Research and development
SEM	Scanning electron microscopy
SCE	Saturated calomel electrode
SHE	Standard hydrogen electrode
SFWS	Spent Fuel and Waste Science and Technology (campaign)
SNF	Spent nuclear fuel

This page is intentionally left blank.

SPENT FUEL AND WASTE SCIENCE AND TECHNOLOGY CAMPAIGN

1. INTRODUCTION

The purpose of this project is to develop, test and implement a process model for the degradation rate of spent nuclear fuel that can be readily incorporated into the generic disposal system analyses (GDSA) performance assessment (PA) code to provide reliable radionuclide source terms over the service life of a deep geologic repository. The fuel matrix degradation (FMD) model (or FMDM), which is an electrochemical reactive-transport model based on fundamental redox kinetics and thermodynamics, was developed for this purpose and is currently being updated and tested. The FMD model was originally based the Canadian Mixed Potential Model (CMPM) of Shoesmith and King, 1998, and King and Kolar 2003 but has been expanded to account for key phenomena and customized for application in the ongoing spent fuel and waste science and technology (SFWS) campaign.

The continuing development and implementation of the FMD model address two high level Features, Events, and Processes (FEPs) that are recognized as high R&D priorities for the SFWS campaign (Wang et al., 2014). The FEPs addressed by this model are 2.1.02 (waste form) and 2.1.03 (waste container), which correspond to the high priority research topics P19 (Development of waste form degradation model) and P20 (Development of new waste package concepts and models for evaluation of waste package performance for long-term disposal) identified by Wang et al., 2014.

Specifically, the FMD model uses mixed potential theory to calculate the degradation rate of UO_2 by accounting for all major anodic and cathodic interfacial reactions. Other major phenomena accounted for in the FMD model include:

- effect of hydrogen generated from steel corrosion within a breached waste package,
- alpha radiolysis and the generation of radiolytic oxidants as a function of fuel burn-up,
- Growth a porous layer of uranyl oxyhydroxide and/or uranyl peroxide corrosion phases.
- Complexation of dissolved uranium by carbonate.
- temperature variations of reaction rates (by Arrhenius equations),
- one-dimensional diffusion of all chemical species to and from the fuel and steel surfaces.

The most important process that the FMD model accounts for that was not addressed in the original CMPM is the oxidation of dissolved hydrogen at the spent fuel surface (Jerden et al., 2015). Leaching experiments with spent fuel and simulated spent fuel have shown that the presence of hydrogen generated during the corrosion of steel added to a test can decrease the fuel degradation rate by 4 orders of magnitude relative to tests performed with no steel present (e.g., Röllin et al., 2001, Ollila, 2008). The means by which the effect of hydrogen is accounted for in the FMD model is discussed in Section 2 below.

Jerden et al., 2017(a) and Jerden et al., 2017(b) discussed the addition of a corroding steel surface as a source of hydrogen to the FMD model (FMDM version 3). One of the main findings of that work is that the extensive coupling between the corrosion of waste package components and the spent fuel that must be taken into accounted to accurately predict radionuclide source terms. As discussed in Jerden et al., 2017(b), the Eh and pH conditions within a breached waste package will evolve with time due to coupled reactions of alloy corrosion, radiolysis, and spent fuel dissolution. The latest FMD model includes a first step towards accounting for coupled processes by linking steel corrosion kinetics and fuel degradation rates; however, more extensive experimental and modeling work is needed to accurately model the fuel dissolution rate because the in-package solution chemistry evolves due to the corrosion of engineering materials.

The present report updates the work discussed in Jerden et al., 2017(a) and Jerden et al., 2017(b) and provides discussion of ongoing experimental validation work for the latest version of the FMD model (FMDM version 4). The electrochemical experiments that are being performed to parameterize and validate the FMD model (V.4) are discussed in Section 3 below.

As summarized in Jerden et al., 2017(b), the FMD model has been successfully integrated with the GDSA-PA code PFLOTRAN; however, there is a need to optimize the integrated code to improve computing speed. This optimization work is ongoing and will be summarized in a March 2019 milestone report The flow of information within the integrated FMDM – GDSA-PA model is summarized in Figure 1.

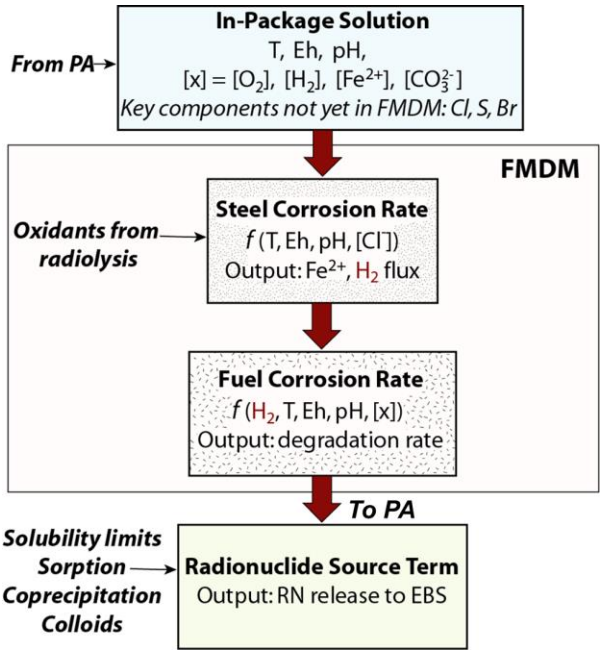

Figure 1. Summary figure showing the context of the FMDM within the source term calculation information flow (adapted from Jerden et al., 2017a).

2. UPDATE ON VALIDATION OF FUEL MATRIX DEGRADATION MODEL VERSION 4

The chemical and physical processes accounted for in the FMD model are shown schematically in Figure 2. In The model, spent fuel is exposed to an aqueous solution that has entered the waste package following a canister breaching event. The model conservatively assumes that the Zircaloy fuel cladding (not shown in Figure 2) is also breached at the time of water infiltration into the canister. The canister breaching process will be modeled separately; however, the breaching model will be coupled with the FMDM through the dependence of the spent fuel degradation rate on the concentration of hydrogen generated from the corrosion of canister steels.

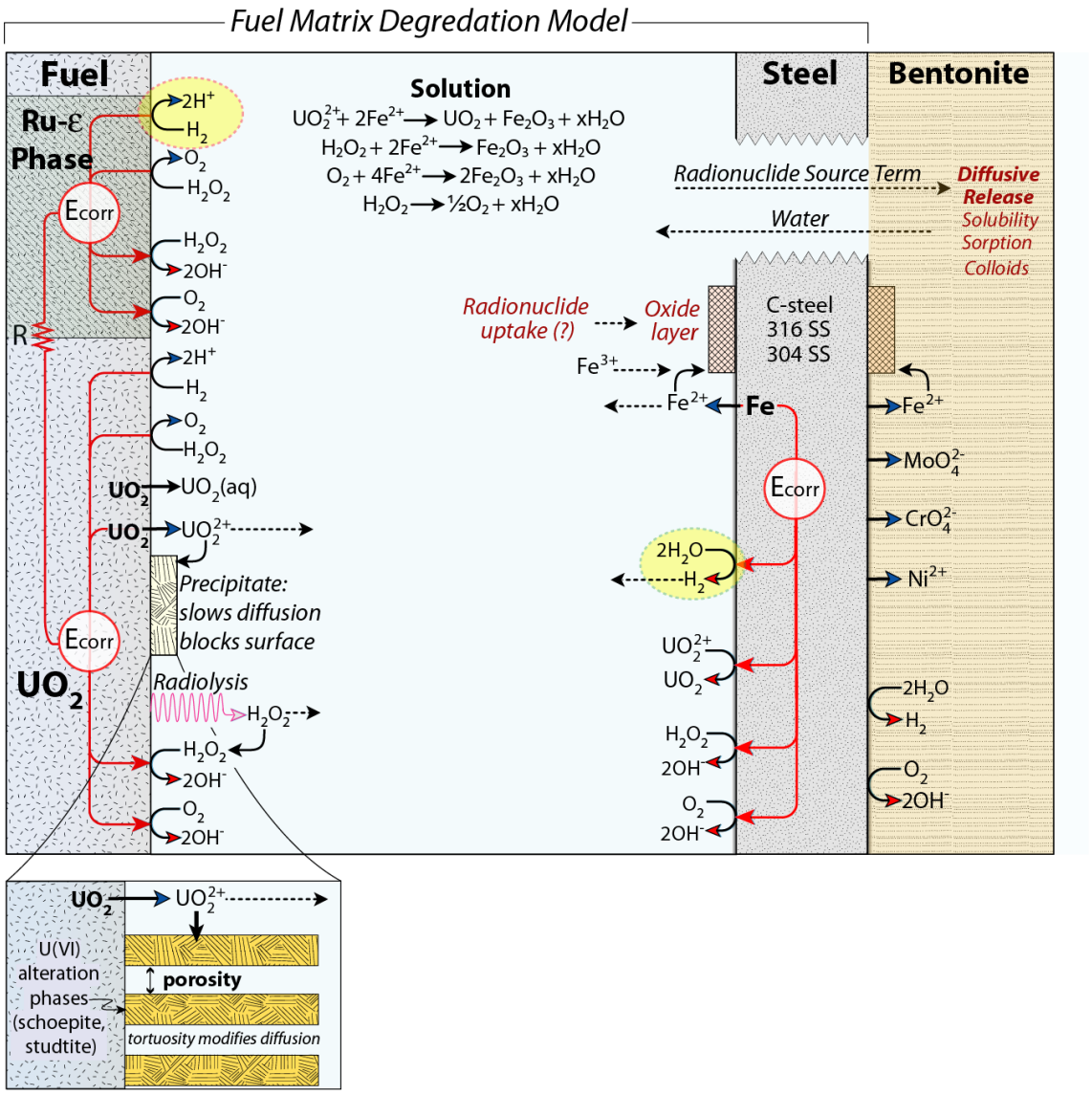

Figure 2. Schematic diagram showing the reaction scheme for the FMD model and identifying other key processes that influence in-package chemistry and radionuclide mobilization. (adapted from Jerden et al., 2017a).

Of the processes shown in Figure 2, H_2 generation and oxidation reactions (highlighted in yellow in Figure 2) have the most important impact on the fuel dissolution rate and radionuclide source term (Jerden et al. 2015). In the absence of H_2 generation, the dominant process is the oxidative dissolution of the fuel by the radiolytic oxidant H_2O_2 and its decomposition product O_2. In the FMD model, the H_2O_2 concentration is calculated using an analytical form of the radiolysis model developed at PNNL (Buck et al., 2014) and the burn-up/dose rate function that was derived from MCNPX dose rate modeling of Radulescu, 2001.

When sufficient H_2 is present, the radiolytic oxidation of the fuel is counteracted by the oxidation of H_2 at the fuel surface. As shown in Figure 2, hydrogen oxidation occurs both on the UO_2 surface and on the Ru-Mo-Pd-Rh-Tc bearing, fission product alloy commonly referred to as the ε phase. The reaction of H_2 with the ε phase is the dominant mechanism for the H_2 effect on spent fuel dissolution due to the catalytic properties of this noble metal-bearing phase. The assumption that the ε phase catalyzes H_2 oxidation at the fuel surface is supported by the electrochemical experimental work of Broczkowski et al., 2005 and Shoesmith, 2007. Their results, which are summarized in Figure 3, show that the presence of dissolved H_2 lowered the corrosion potential of simulated spent fuel specimens containing the ε-phase relative to specimens that did not contain ε phase particles. Furthermore, increasing the amount of ε-phase in the specimens (simulating higher burnup: BU 2% vs 6% in Figure 3) further decreased the measured corrosion potential for the same H_2 concentration.

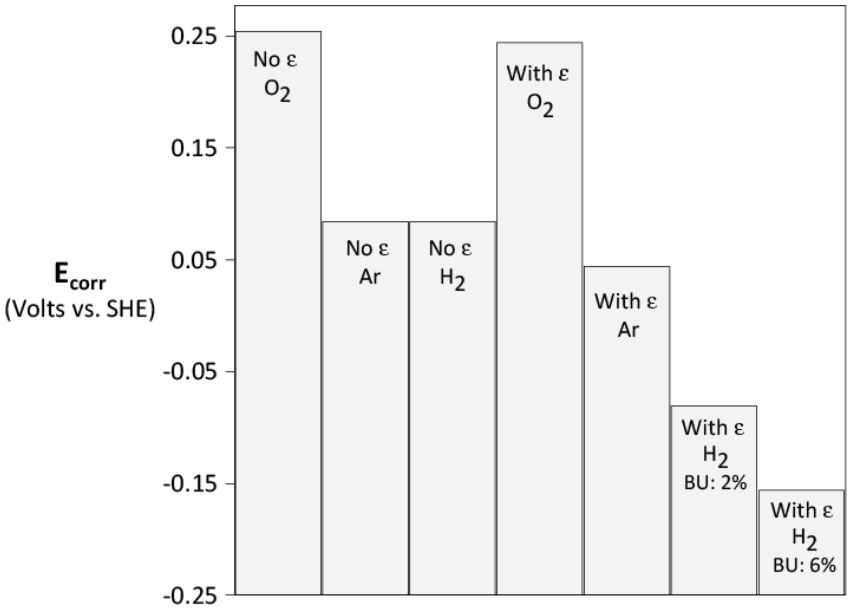

Figure 3. Summary of results from Shoesmith, 2008 showing measured corrosion potentials for simulated spent fuel specimens with and without the fission product alloy Ru ε-phase. The conditions for the tests included bubbling either O_2, Ar or a gas mixture of 5% H_2 in Ar through the electrochemical cell solution. All tests were at 60°C. BU denotes simulated burnup, where higher burnup indicates a higher surface area coverage of the ε-phase (adapted from Shoesmith, 2008).

The FMD model calculates the net effect of all redox reactions occurring in the system based on the fuel and steel corrosion potentials (E_{corr}). The corrosion potential is the voltage at which the rates of the anodic and cathodic reactions are equal, that is, at E_{corr} the anodic dissolution current density is balanced by the cathodic oxidant reduction current density (participating reactions are shown schematically in red on Figure

2). Steel corrosion rate at the E_{corr} value established by a particular environmental condition (Eh, pH, chemistry) will depend on whether it corrodes actively or passivates. Under anoxic conditions, the steel corrosion rate is directly proportional to the rate of H_2 generation at the steel surface, since the only cathodic reaction occurring under anoxic conditions is the reduction of water to form H_2. The corrosion rate can be measured electrochemically as a corrosion current, which can be converted to a surface area-normalized mass dissolution rate by using Faraday's law for implementation in the FMD model.

All of the processes shown in Figure 2 are quantified in a parameter database that is updated as new experimental results are obtained. The FMD model parameter database is summarized in Table 1 and the specific parameters updated for FMDM V.4 are shown in Table 2.

Table 1. Summary of FMDM parameters and data gaps that need to be addressed in experimental work to improve the accuracy of the model (adapted from Jerden et al., 2017b).

Parameter	Description	Data needs to improve accuracy
Dimension of fuel environment	(mm – cm)	To be updated when dimensions of waste package are known
Nodes in fuel environment	(log-space grid: fine-spacing near surface)	To be updated when dimensions of waste package are known
Fuel surface coverage by NMP	(~1%)	From literature
Dimension of steel environment	(mm – cm)	To be updated when dimensions of waste package are known
Nodes in steel environment	(log-space grid: fine-spacing near surface)	To be updated when dimensions of waste package are known
Number of FMDM time steps	(100 – 1000)	Use to optimize PA interface
Fuel alteration layer porosity	(~50%)	From literature
Fuel alteration layer tortuosity	(~0.01)	From literature
Fuel alteration layer radiolysis factor	(*not used*)	*Could be activated to account for radionuclide uptake by U secondary phases*
Alpha particle penetration depth	(35μm)	From literature
Fuel burnup	(25 – 75 GWd/MTU)	**Input from PA**
Age of fuel (time out of reactor)	30 – 100 yrs	**Input from PA**
Resistance between fuel and NMP domains	(10^{-3} Volts/Amp)	Interpretation of literature
Temperature history	function	**Input from PA**
Dose rate history	function	Based on MCNPX results of Radulescu, 2011
Spatial dose rate	function (decrease in dose rate with distance from fuel)	Based on MCNPX results of Radulescu, 2011
Rate constants for interfacial reactions in fuel and steel domains	See Figure 2 for summary of specific reactions	**Data need:** experiments needed due to lacking or inconsistent data in current literature on H_2 reactions on fuel and NMP and steel corrosion under relevant conditions
Charge transfer coefficients for interfacial half-cell reactions in fuel and steel domains	See Figure 2 for summary of specific reactions	**Data need:** experiments needed due to lacking or inconsistent data in current literature on H_2 reactions on fuel and NMP
Activation energies	T dependence: See Figure 2 for summary of specific reactions	**Data need:** experiments needed due to lacking or inconsistent data in current literature on H_2 reactions on fuel and NMP and steel corrosion under relevant conditions

Table 1. Continued.

Parameter	**Description**	**Data needs to improve accuracy**
Standard potentials for interfacial half-cell reactions: fuel and steel	See Fig. 2 for reactions	From literature
Relative area of fuel domain	Default 1:1, depends on waste package design	To be updated when dimensions of waste package are known
Relative area of steel domain	Default 1:1, depends on waste package design	To be updated when dimensions of waste package are known
Environmental leak rate (diffusion barrier factor)	Depends on waste package design, breach	Interpretation of literature
Environmental concentrations	(O_2, H_2, CO_3^{2-}, Fe^{2+}, Cl^-)	**Input from PA**
Rate constants for bulk solution reactions in fuel, steel environments	See Figure 6 for summary of specific reactions	From literature
Activation energy for bulk solution reactions	T dependence, See Figure 8 for reactions	From literature
Passivation potential of steel surface	(75 V_{SCE}) as place-holder	**Data need:** experiments needed due to lacking or inconsistent data in current literature. For example, C-steels may not passivate under repository relevant conditions. More data are needed to determine active corrosion rates and to quantify the role magnetite corrosion layers play in corrosion behavior at pH > 8.
Passivation corrosion current density	Calculated internally within FMDM	**Data need:** experiments needed due to lack of data in literature
Radiolytic oxidant (H_2O_2) generation value (G_{cond})	Analytical function for conditional G_{H2O2} value from PNNL radiolysis model	Values based on radiolysis model results, Buck et al., 2013. *Would need to be updated, expanded for brine solutions (Cl, Br)*

Table 2. Specific electrochemical parameters that are dominant in determining the rate of spent fuel degradation in the FMD model. The rate constants for the reduction of H_2O_2 and O_2 (bold) are newly updated values for the FMDM V.4, while all others are the same as FMDM V.3. The V.3 parameters were derived from King and Kolar 2004 except for the steel corrosion parameters which are alloy specific and need to be determined experimentally.

Reactions	**Equation**	**k*** (mol m^{-2} s^{-1} or mol s^{-1})	**α**	**E^0** (V)
$UO_2 \xrightarrow{k_{UO_2}} UO_2^{2+} + 2e^-$	$i^{UO_2} = nAFk_{UO_2}\exp\left[\frac{\alpha_{UO_2}F}{RT}(E_{corr}^{UO_2} - E_{UO_2}^0)\right]$	$5.0x10^{-8}$	0.96	0.17
$H_2 + 2OH^- \xrightarrow{k_{H_2}} 2H_2O + 2e^-$	$i^{H_2} = nAFk_{H_2}\exp\left[\frac{\alpha_{H_2}F}{RT}(E_{corr}^{\varepsilon-phase} - E_{H_2}^0)\right]$	$1.0x10^{-3}$	0.5	0.58
$H_2O_2 + \xrightarrow{k_{H_2O_2}} O_2 + 2H^+ + 2e^-$	$i^{H_2O_2} = nAFk_{H_2O_2}\exp\left[\frac{\alpha_{H_2O_2}F}{RT}(E_{corr}^{UO_2} - E_{H_2O_2}^0)\right]$	$7.4x10^{-10}$	0.41	0.12
$H_2O_2 + 2e^- \xrightarrow{k_{H_2O_2}} 2OH^-$	$i^{H_2O_2} = nAFk_{H_2O_2}\exp\left[\frac{\alpha_{H_2O_2}F}{RT}(E_{corr}^{UO_2} - E_{H_2O_2}^0)\right]$	**$2.0x10^{-14}$**	-0.41	0.97
$O_2 + 2H_2O + 4e^- \xrightarrow{k_{O_2}} 4OH^-$	$i^{O_2} = nAFk_{O_2}\exp\left[\frac{\alpha_{O_2}F}{RT}(E_{corr}^{UO_2} - E_{O_2}^0)\right]$	**$1.0x10^{-12}$**	-0.50	0.43
$Fe \xrightarrow{k_{Steel}} Fe^{2+} + 2e^-$	$i^{Steel} = nAFk_{Steel}\exp\left[\frac{\alpha_{Steel}F}{RT}(E_{corr}^{Steel} - E_{Steel}^0)\right]$	*Data Need*	*Data Need*	*Data Need*
$2H_2O + 2e^- \xrightarrow{k_{H_2}} H_2 + 2OH^-$	$i^{H_2O} = nAFk_{H_2O}\exp\left[\frac{\alpha_{H_2O}F}{RT}(E_{corr}^{Steel} - E_{H_2O}^0)\right]$	$5.0x10^{-7}$	-0.48	-1.1

Where (i) is the current density for a half-call reaction (proportional to the reaction rate), (k) is the half-cell reaction rate constant, (α) is the charge transfer coefficient and (E^0) is the standard potential.

#Values shown in bold are updated constants for FMDM V.4 that were derived by comparing the FMDM results to experimental data (see Figure 4 and 5).

*The rate constant and other parameter values for steels will vary depending on the alloy composition. Electrochemical experiments with relevant alloys such as 316, 304 and low carbon steels are needed to quantify these parameter values.

As indicated in Table 2, the parameter values that were updated for FMDM V.4 are the rate constants for the reduction of H_2O_2 and O_2 on the UO_2 surface. These rate constants are used in the Butler Volmer relationships on which the FMD model is based on (see Table 2 for details).

The comparison of model results from FMDM V.4 and experimental datasets for the dissolution rate of spent fuel, simulated spent fuel and UO_2 are shown in Figures 4 and 5. The purpose of the comparison of the FMD model results to the experimental data was not to fit the data in a statistical sense, but rather to improve the accuracy of the model results while maintaining a conservative margin of safety (i.e. model should reasonably overpredict degradation rates). As shown in Figure 3 the newer parameter value for the H_2O_2 reduction give a more accurate conservative bound to the experimental data.

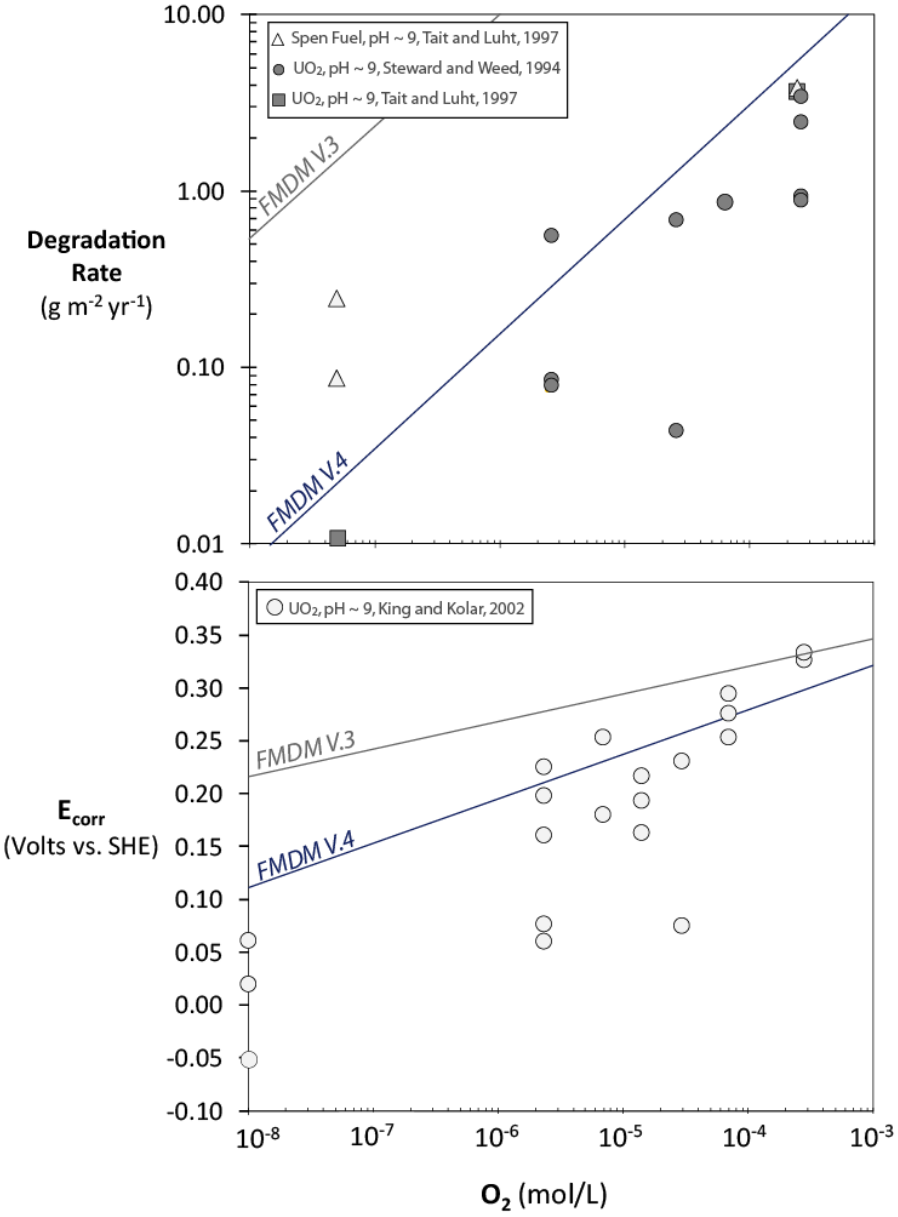

Figure 4. Comparison of results from the updated version 4 of the FMD model to experimental results. The model runs were for 25ºC and no other oxidants were present.

Figure 4 shows the degradation rate (top plot) and E_{corr} (bottom plot) calculated by the FMDM V.3 and FMDM V.4 over a range of relevant dissolved concentrations of O_2 (no other oxidants present) and compares the model results to experimental data. The comparisons show that FMDM V.4 with the updated parameter value for O_2 reduction on the fuel (Table 2) is more consistent with the experimental results. The data points for spent fuel at ~$5x10^{-8}$ M O_2 in the degradation plot (top) are elevated relative to the general trend in the data due to the presence of radiolytic oxidants other than O_2 in those tests.

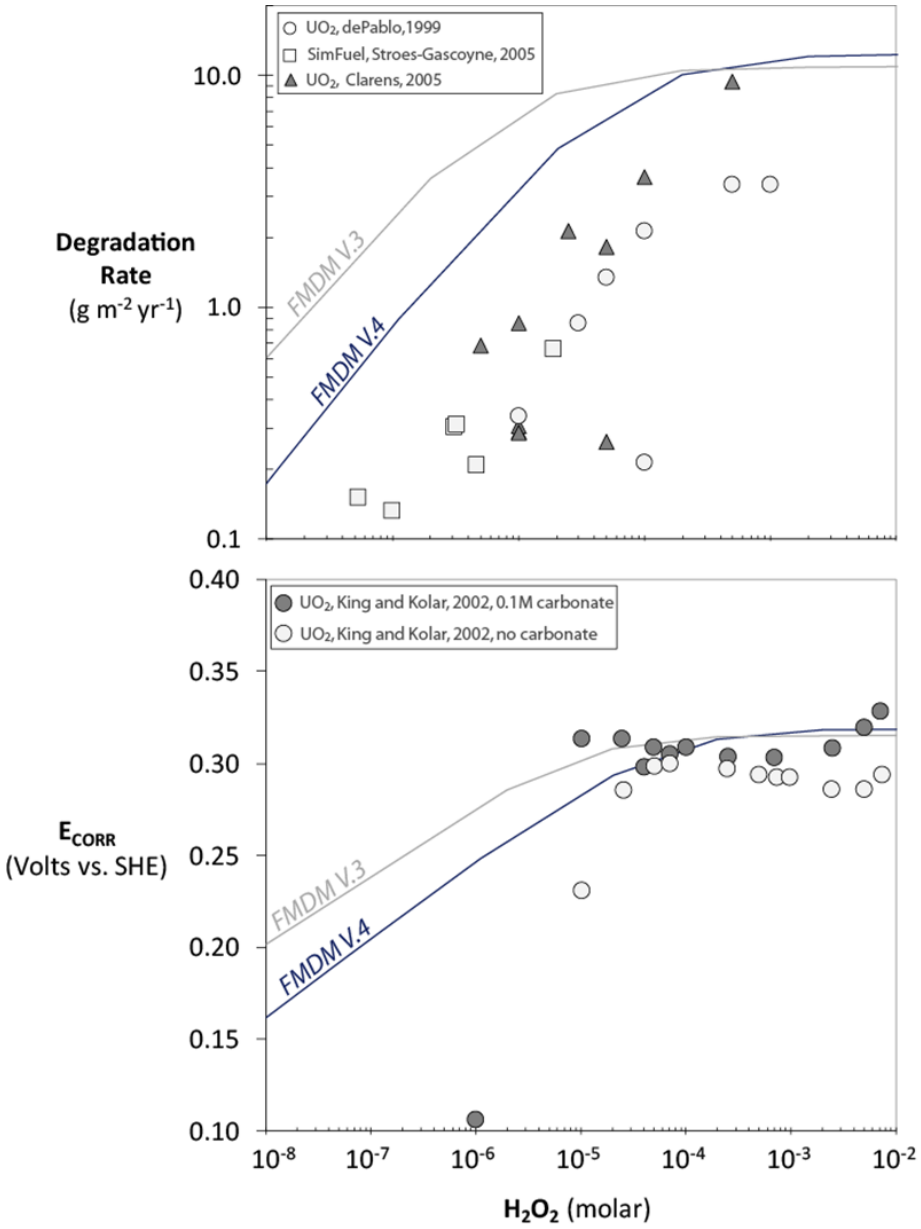

Figure 5. Comparison of results from the updated version 4 of the FMD model to experimental results. The model runs were for 25ºC and an O_2 concentration of 10^{-9} molar.

Figure 5 shows the degradation rate (top plot) and E_{corr} (bottom plot) calculated by the FMDM V.3 and FMDM V.4 over a range of relevant dissolved concentrations of H_2O_2 and compares the model results to experimental data. In general, the FMDM V.4 with the updated parameter value for H_2O_2 and O_2 reduction on the fuel (Table 2) is more consistent with the experimental results. The model results for the degradation rate (top plot) are purposefully high as the goal is for the model to provide a conservative, but realistic, upper bound for the spent fuel dissolution rate.

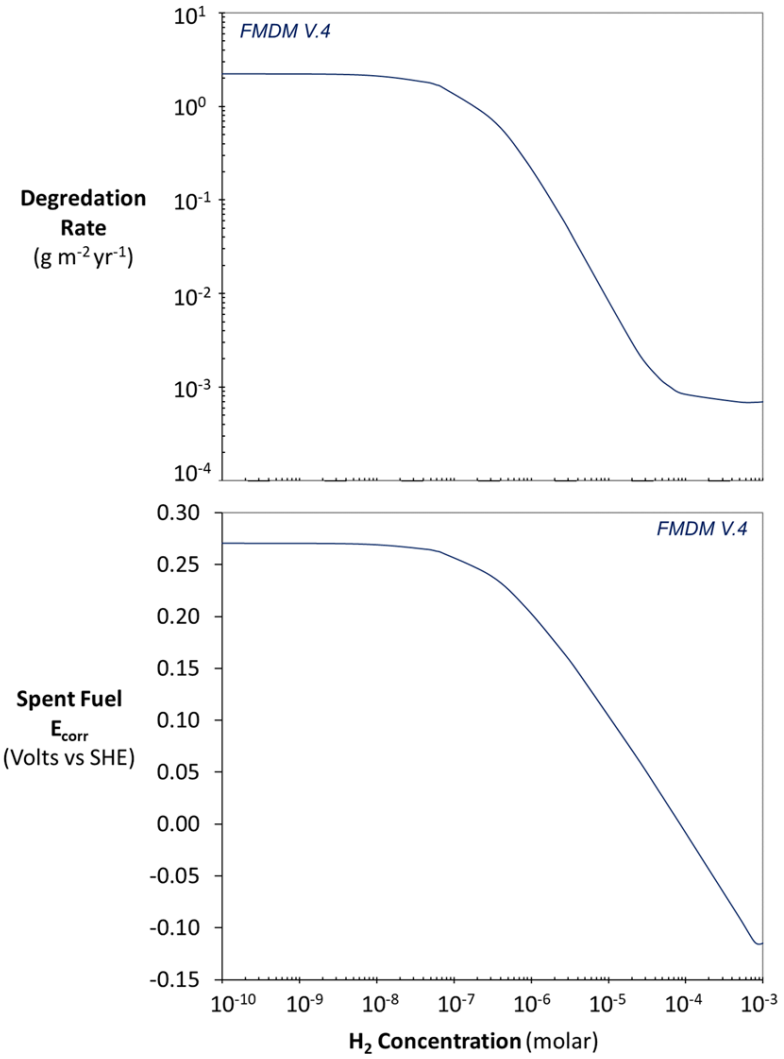

Figure 6. Results from version 4 of the FMD model showing the degradation rate and calculated E_{corr} as functions of the H_2 concentration at the spent fuel surface. For these runs the temperature was 25°C, the O_2 concentration was 10^{-9} M and the H_2O_2 concentration was 10^{-6} M.

Figure 6 shows the degradation rate (top plot) and E_{corr} (bottom plot) calculated by the FMDM V.4 over a range of relevant dissolved concentrations of H_2 concentrations at the spent fuel surface. The degradation plot (top) shows an inflection around 10^{-7} M H_2 indicating that the oxidation of H_2 begins to counteract the oxidative dissolution of the fuel at sub micromolar concentrations. When the H_2 concentration increases to around 10^{-4} M, the oxidation of H_2 becomes the dominant anodic reaction at the fuel surface thus effectively shutting off oxidative dissolution. Under the conditions for this model run the threshold E_{corr} for effectively shutting down the oxidative dissolution of the fuel is around 0.0 volts vs. SHE. As shown in Figure 6, after oxidative dissolution is shut down by H_2 oxidation the fuel continues to degrade at a rate of approximately 10^{-3} g m^{-2} yr^{-1}, which is the chemical dissolution rate of the fuel [UO2(s) → UO_2(aq)]. This lower degradation rate value is consistent with experimental results under reducing conditions (Jerden et al., 2017a).

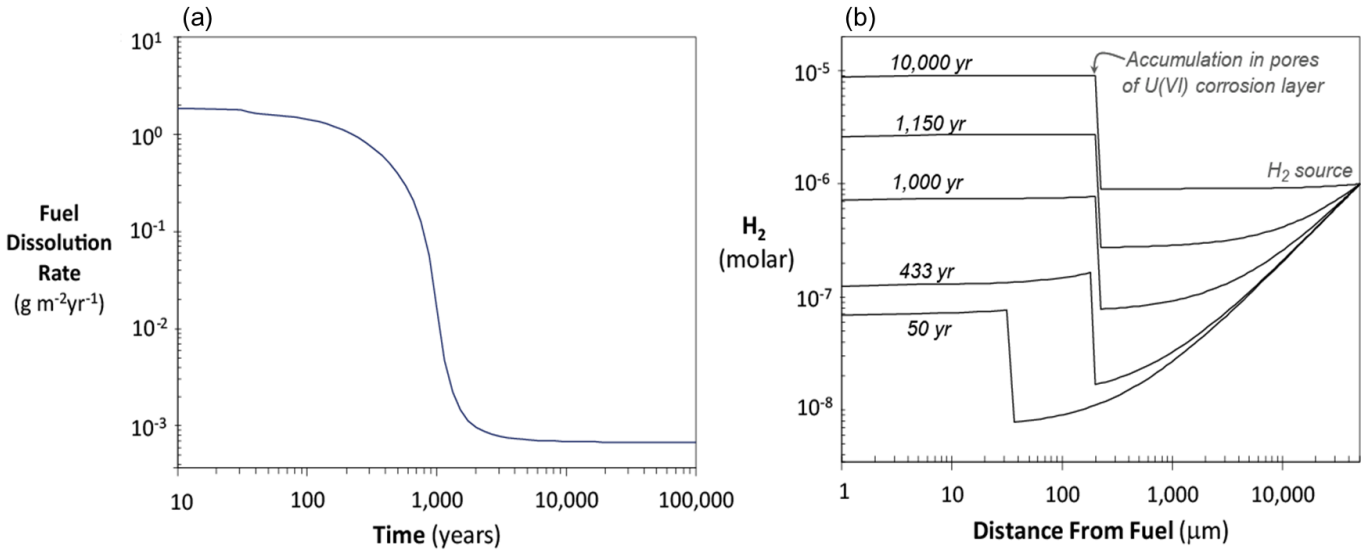

Figure 7. Model results using FMDM V.4 showing the fuel degradation rate as a function of time (a) and the H_2 concentration as a function of distance from the fuel surface (b). The temperature for these model runs was 25°C, the O_2 concentration was 10^{-9} M and the fuel burnup was 60 GWd/MTU.

Figure 7 shows the fuel degradation rate vs. time (a) and the H_2 concentration profiles at several times during a typical repository simulation. This example indicates the importance of the accumulation of H_2 near the fuel surface with time. This accumulation is accentuated by the presence of the porous U(VI) corrosion layer, which is modeled as a set of parallel tortuous pores that decrease species diffusion rates. In this example, a concentration of around $3x10^{-6}$ M H_2 is sufficient to counteract the oxidative dissolution of the fuel; however, this concentration is not achieved until around 1200 years. The H_2 source in this example is assumed to be a constant concentration of $1x10^{-6}$ M; however, in more realistic scenarios the H_2 source concentration will change depending on how changing repository conditions determine steel corrosion rates as a function of time. The addition of the steel corrosion module into the FMD model and the associated validation experiments will allow for the modeling of this more realistic scenario.

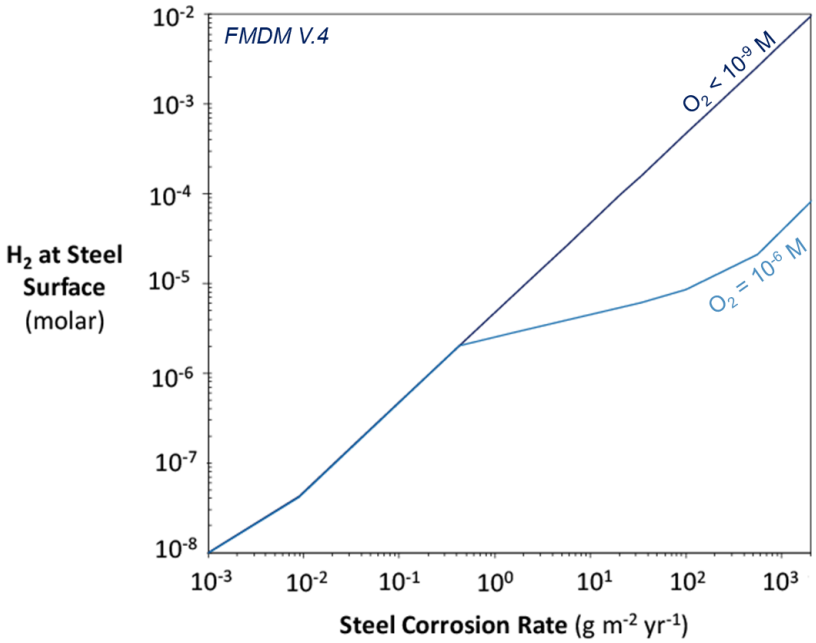

Figure 8. Model results using steel corrosion module of the FMDM V.4 showing the calculated H_2 concentration at the fuel surface as a function of the steel corrosion rate. The temperature for these model runs was 25°C, the O_2 concentration was 10^{-9} M and the O_2 concentration is indicated on the plot.

Figure 8 shows the concentration of H_2 produced by steel corrosion calculated by the steel corrosion module of the FMDM V.4 for different starting O_2 concentrations. This plot indicates how changes in dissolved oxygen concentrations can significantly affect the amount of H_2 produced by steel corrosion. For example, for a steel corrosion rate of around 100 g m^{-2} yr^{-1} and nanomolar O_2 the H_2 concentration due to steel corrosion would be around $5x10^{-4}$ M vs. a H_2 concentration of around $9x10^{-6}$ for solutions containing micromolar O_2. As shown in Figures 6, a concentration of $5x10^{-4}$ M H_2 is more than enough to shut down the oxidative dissolution of the fuel, while concentrations around 10^{-5} M H_2 do not completely counteract oxidative fuel degradation for 60 GWd/MTU fuels that are less than 1000 years old. Figure 8 highlights the need for an accurate and experimentally validated steel corrosion model that will provide a way to account for different alloy corrosion rates (i.e. different H_2 source concentrations) under changing repository conditions.

3. ELECTROCHEMICAL EXPERIMENTS TO PARAMETERIZE THE FMDM STEEL CORROSION MODULE

3.1. Background

As discussed above, establishing accurate steel corrosion rates for relevant disposal conditions is essential for accurate spent fuel degradation and source term modeling because of the dominant effect of H_2 on the spent fuel dissolution rate (as shown in Figures 6 and 7 above). The half-cell reactions of particular interest for H_2 generation are as follows:

$Fe^0 \rightarrow Fe^{2+} + 2e^-$ (Reaction 1)

$2H_2O + 2e^- \rightarrow H_2 + 2OH^-$ (Reaction 2a)
$2H^+ + 2e^- \rightarrow H_2$ (Reaction 2b)

with the overall steel corrosion reactions

$Fe + 2H_2O \rightarrow H_2 + Fe^{2+} + 2OH^-$ (Reaction 3a)
$Fe + 2H^+ \rightarrow H_2 + Fe^{2+}$ (Reaction 3b)

Reactions 3b and 3a indicate the fundamental coupling between steel corrosion and H_2 generation in alkaline and acidic conditions (respectively). The oxidation of other steel constituents (e.g., Cr, Mo, Ni, and Mn) will contribute to the anodic current, but the oxidation of Fe will be dominant.

To provide context for the experimental plan, Figure 9, which is a simplified version of the reaction FMDM reaction scheme shown above in Figure 2 above, that highlights the key H_2 consuming and producing reactions and shows schematically the potential importance of Zircaloy cladding as a source of hydrogen. Carbon steels, stainless steels and Zircaloly will all be corroding simultaneously with the spent fuel, therefore, our experiments will include representative specimens of each of these alloy types.

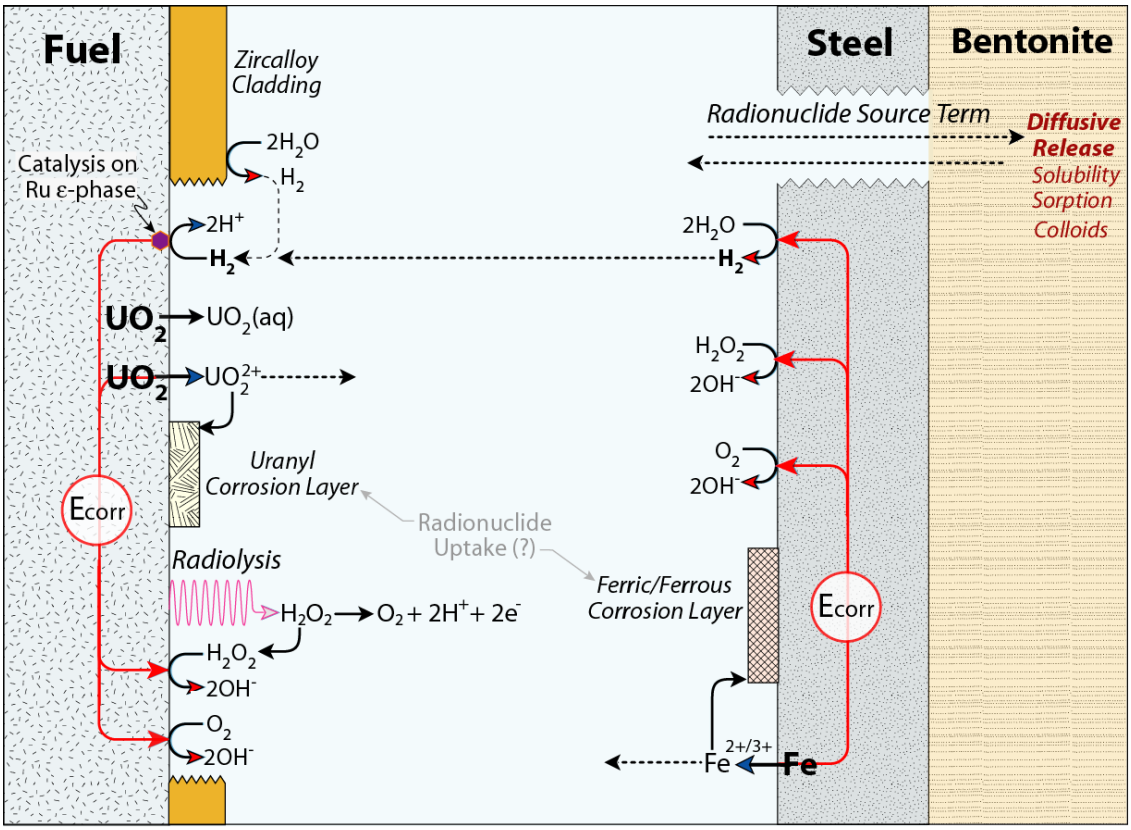

Figure 9. Schematic diagram of the FMD model reaction scheme highlighting the reactions that consume and produce H_2.

As discussed in Jerden et al., 2017(a), there is a wealth of literature on steel corrosion but much of the previous work was not done under conditions relevant for crystalline and argillite rock-type repositories. For example, Arthur has compiled corrosion rate data for a number of relevant alloys tested under a variety of conditions (Table 3); however, this compilation does not include the anoxic corrosion rates that that are more relevant to crystalline and argillite repository concepts. There is a significant amount of literature data on the corrosion of carbon steels, cast iron and forged steels (see reviews by Johnson and King, 2003 and King, 2007); however, much of these corrosion rate data are derived from batch style immersion tests that provide average cumulative rates rather than the instantaneous corrosion rates needed to represent the H_2 generation rates and to parameterize and validate the FMDM steel corrosion module.

Steel coupon immersion tests provide useful information on mineralogy and the evolution of the chemical system, but the Eh, pH and solution chemistry are not controlled and the surface conditions can change significantly over the test duration. Corrosion rates derived from immersion tests are based on cumulative mass loss measurements or corrosion layer thicknesses that do not indicate how the corrosion rate (and thus H_2 generation rate) varies with time or conditions (most importantly, with the solution Eh). Knowing these dependencies of the H_2 generation rate is essential for modeling spent fuel dissolution under evolving in-package chemical conditions.

Electrochemical tests can be used to quantify the effects of surface stabilization due to passivation and localized corrosion, such a pitting, that can only be qualitatively observed in coupon immersion tests. Furthermore, electrochemical methods can measure rates on the order of nanograms cm^{-2} d^{-1}. Thus, the use of electrochemical methods would provide reliable corrosion rates for durable EBS materials (including

Zircaloy cladding) and provide dependencies on environmental conditions that could be used to predict the long-term generation of H_2 and attenuation of fuel degradation rates as the seepage water composition evolves.

Table 3. Statistical summary of immersion-type corrosion test results compiled by Arthur, 2004 (adapted). The anaerobic carbon steel corrosion rates are from King, 2007.

Metal	Conditions	Corrosion Rate (g m^{-2} yr^{-1})				Standard Deviation
		Min	Max	Median	Mean	
Stainless Steel Types 302/304/304L	Dilute groundwater[1] (25°C to 100°C)	0.01	12.56	1.03	1.71	2.38
	Saltwater (26.7°C)	12.70	313.18	40.64	91.53	89.07
	Saltwater (90°C)	5.28	127.20	16.24	46.53	47.62
Stainless Steel Types 316/316L/AM-350	Dilute groundwater (29.5°C)	0.01	0.38	0.02	0.07	0.11
	Dilute groundwater (50°C to 100°C)	0.30	4.08	1.83	1.98	1.17
	Saltwater (26.7°C)	0.01	118.30	5.89	15.51	26.77
Neutronit (borated stainless steel)	Dilute groundwater (29.5°C)	0.01	0.09	0.02	0.03	0.03
	Dilute groundwater (50°C to 100°C)	0.20	2.64	1.62	1.65	0.70
	Saltwater (26.7°C)	14.48	233.76	59.04	88.48	81.52
Stainless Steel Type 304 Alloyed with 0.3% Boron	Dilute groundwater (~25°C)	24.40	97.52	36.56	48.80	30.88
	Dilute groundwater (boiling)	24.40	219.44	134.08	126.00	63.92
Stainless Steel Type 304 Alloyed with 1.5% Boron	Boiling Dilute groundwater	1292.32	2023.84	1694.72	1682.48	262.16
Carbon Steel	Dilute groundwater (60°C)	629.68	1045.60	815.60	821.68	98.96
	Dilute groundwater (90°C)	464.64	1040.16	616.40	649.12	121.04
	Concentrated groundwater (60°C)	402.00	833.60	502.16	544.64	113.36
	Concentrated groundwater (90°C)	59.12	176.48	99.36	102.24	30.16
	Anoxic DIW in bentonite (80°C)	31.6	87.5	NA	NA	NA
	Anoxic brine in bentonite (80°C)	50.3	161.3	NA	NA	NA

[1]Dilute groundwater: dilute simulated ground waters with compositions similar J13 well water, a dilute sodium carbonate groundwater from the Yucca Mountain Site (see Arthur et al., 2004 for composition).
[2]Saltwater refers to sea water with ~17,000 ppm chloride.
[3]Concentrated groundwater: simulated J13 well water concentrated 1000x by evaporation.
NA: not applicable, no statistical analysis performed.

To provide instantaneous corrosion rates under controlled redox conditions, we have initiated a set of electrochemical experiments focused on providing parameter values and validation data for the FMD model for a range of relevant alloys.

3.2. Method and Results

The electrochemical corrosion experiments being performed at Argonne employ the standard three electrode method as described by Bard and Faulkner, 2001. The three-electrode cell used for the Argonne tests consists of a 20 mL jacketed, borosilicate glass vessel with a saturated calomel reference electrode (SCE), a graphite counter electrode and a steel, Zircaloy or UO_2 working electrode. A typical electrochemical cell and working electrode is shown in Figure 10. For these scoping experiments, an aggressive 10 mM NaCl solution adjusted to pH 4 with sulfuric acid was used as the electrolyte.

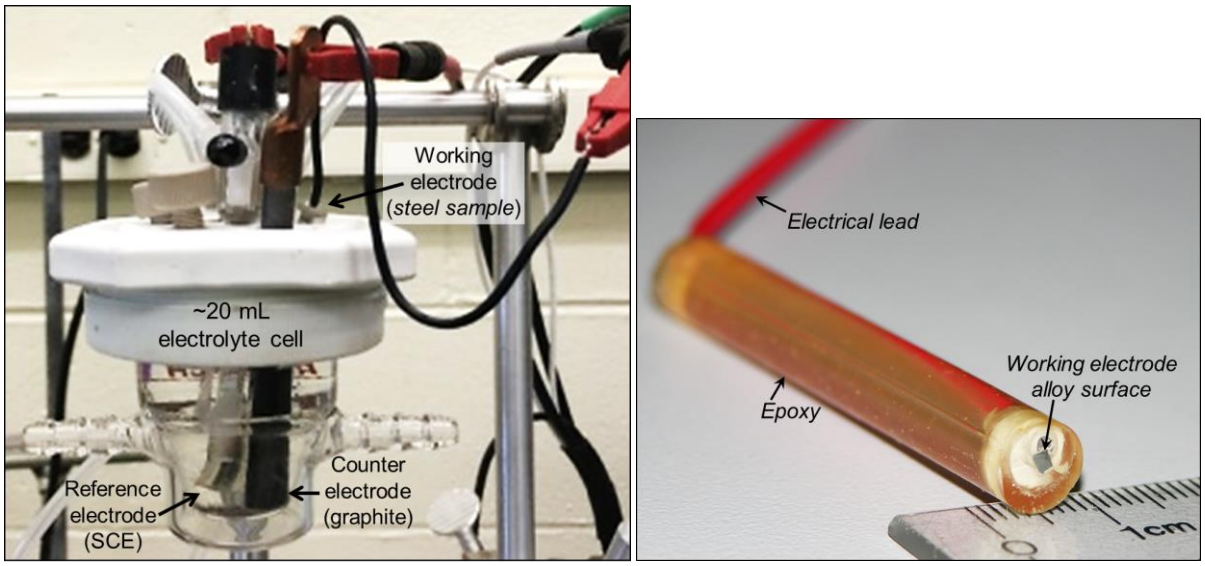

Figure 10. Three-electrode electrochemical cell used in Argonne electrochemical experiments (left) and an example alloy working electrode (right). The working electrode shown is made of Zircaloy-4, but the steel electrodes used for ongoing and future tests are the same size and mounted in the same way.

In the electrochemical tests, the electrolyte is used to impose chemical effects, including pH and Cl^- concentrations, and a potentiostat is used to impose a surface potential representing the solution Eh. The potentiostat can be used to impose a wide range of fixed potentials to efficiently determine the effect of the solution Eh on the steel corrosion and H_2 generation rate. In practice, a potentiodynamic scan is performed to measure E_{corr} for the polished surface in the test solution and identify regions of active and passive behavior to be studied in subsequent potentiostatic tests. The potentiodynamic scan indicates the propensity for active or passive corrosion, but the rapid scan rate does not allow stable passive layers to form. Potentiostatic tests are conducted to measure the corrosion currents as stable passive layers form or the constant currents are achieved with actively corroding metals.

Figure 11 (adapted from Jerden et al., 2017a) shows typical results for potentiodynamic (PD) scans (a) and potentiostatic (PS) measurements (b) in tests with the three main alloys of interest. These scoping tests were performed under aggressive corrosion conditions (pH 4 for steels and pH 1 for Zircaloy) to optimize the methodology. These types of PD and PS analyses will be performed under a range of relevant repository conditions as part of the ongoing FY18 and future FY19 electrochemical tests. The test matrix for these ongoing and planned experiments is shown in Table 5.

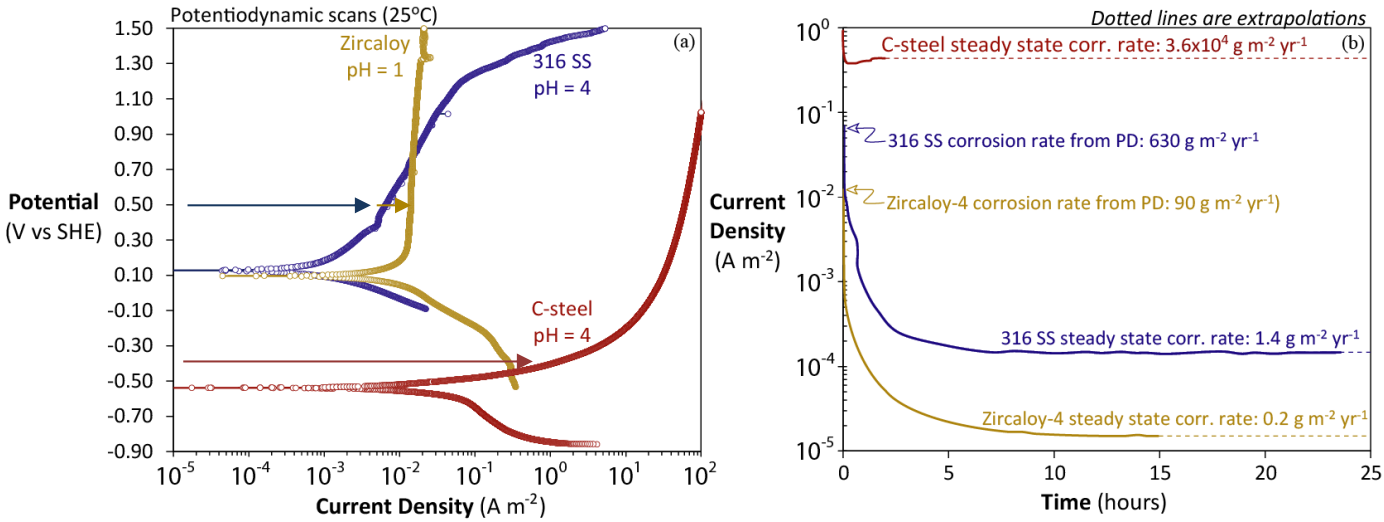

Figure 11. Example data from Jerden et al., 2017(a) showing they types of results obtained from electrochemical measurements: (a) potentiodynamic polarization and (b) potentiostatic corrosion of carbon steel at -0.4 V_{SHE} and pH = 4, 316L stainless steel at 0.5 V_{SHE} and pH = 4, and Zircaloy-4 at 0.5 V_{SHE} in pH 1 solution. The current densities measured in the PD scans are shown in (b) to illustrate the passive stabilization of 316 SS and Zircaloy-4 under these test conditions.

As shown in the scoping test data (Figure 11a) carbon steel, stainless steel and Zircaloy show significantly different corrosion behaviors (Jerden et al., 2017a). Carbon steel corrodes actively at very low potentials and does not passivate; while, stainless steel and Zircaloy-4 are noble at potentials below about -0.2 V and 316L passivates at moderate potentials, but corrodes actively above about 0.5 V. Zircaloy-4 passivates to high potentials in the absence of chloride (as shown), but passivation breaks down in the presence of even small amounts of chloride. As indicated by the arrows in Figure 11a, the potentiostatic tests (Figure 11b) were conducted at potentials above the E_{corr} values. The corrosion currents in the tests with Zircaloy-4 and 316L decrease as the surfaces are rapidly passivated in the pH 4 solution. Relative to the currents measured for the freshly polished clean surfaces in the potentiodynamic scans, the corrosion currents for Zircaloy-4 and 316L decrease about 1.5 and three orders of magnitude due to passivation, respectively. The initial corrosion rate of 316 SS is 630 g m^{-2} yr^{-1} (measured in the PD scan) but the steady state rate of the stabilized surface appropriate for calculating H_2 generation in the FMDM is only 1.4 g m^{-2} yr^{-1}. This rate is consistent with the 316 corrosion rates of 0.01 – 0.38 g m^{-2} yr^{-1} measured in dilute groundwater compiled by Arthur, 2004 (Table 3).

As pointed out in Jerden et al., 2017(a), the corrosion currents measured for the stabilized surfaces (Figure 11b) are appropriate for modeling the long-term H_2 generation rates in the FMD model. These passivated rates for Zircaloy-4 and 316L are readily measured electrochemically, but these are too low to have been measured by mass loss in coupon immersion tests. The corrosion behaviors and rates will be different under different environmental conditions, particularly for different Eh, pH, and Cl^- concentrations, and the differences must be taken into account in the FMD model. The electrochemical tests can provide the rate dependencies on these and other environmental variables.

Representative data from the solids characterization of corrosion phases produced during potentiostatic tests with 4320 carbon steel are shown in Figures 12 and 13. Figure 12 shows SEM micrographs of the freshly polished electrode surface (a) and (b) and the surfaces after potentiostatic corrosion at -0.45 V_{SCE} for different durations (c) and (d). The two distinct phases have different corrosion behaviors. The darker

colored ferrite phase is the common body-centered cubic iron allotrope (α-iron) that corrodes preferentially relative to the lighter colored pearlite, which is a two-phased, lamellar structure consisting of alternating layers of ferrite and a corrosion resistant iron carbide phase (Fe_3C). characterizing the steel microstructure is essential to understanding the corrosion behavior.

The 4320 alloy produced enough oxide corrosion products under the aggressive corrosion conditions (pH 4, potentiostatic holds at 0.1 and -0.45 V_{SCE}) for powder XRD analysis to be performed, and the results are shown in Figure 13. The major mineral phases identified in the corrosion layer were the ferric oxy-hydroxides maghemite (γ-Fe_2O_3) and lepidocrocite [γ-FeO(OH)]. For this experiment, ferric corrosion phases were favored over ferrous phases due to the presence of O_2 in the electrolyte solution. Future tests will focus on lower potentials and lower dissolved O_2 concentrations that are more representative of the reducing conditions anticipated to prevail within crystalline and argillite rock type repositories. A controlled atmosphere glovebox has been constructed to provide a low-oxygen environment for the electrochemical tests.

Most electrochemical tests will not generate enough corrosion phases for phase identification by powder XRD; therefore, electron diffraction by TEM may be used to characterize corroded alloys for selected tests. The TEM samples will be prepared using Argonne's FEI Strata 400 focused ion beam, field emission microscope with an AutoProb 200 sample extraction system (FIB). Specimens will be provided to collaborators within the SFWD campaign.

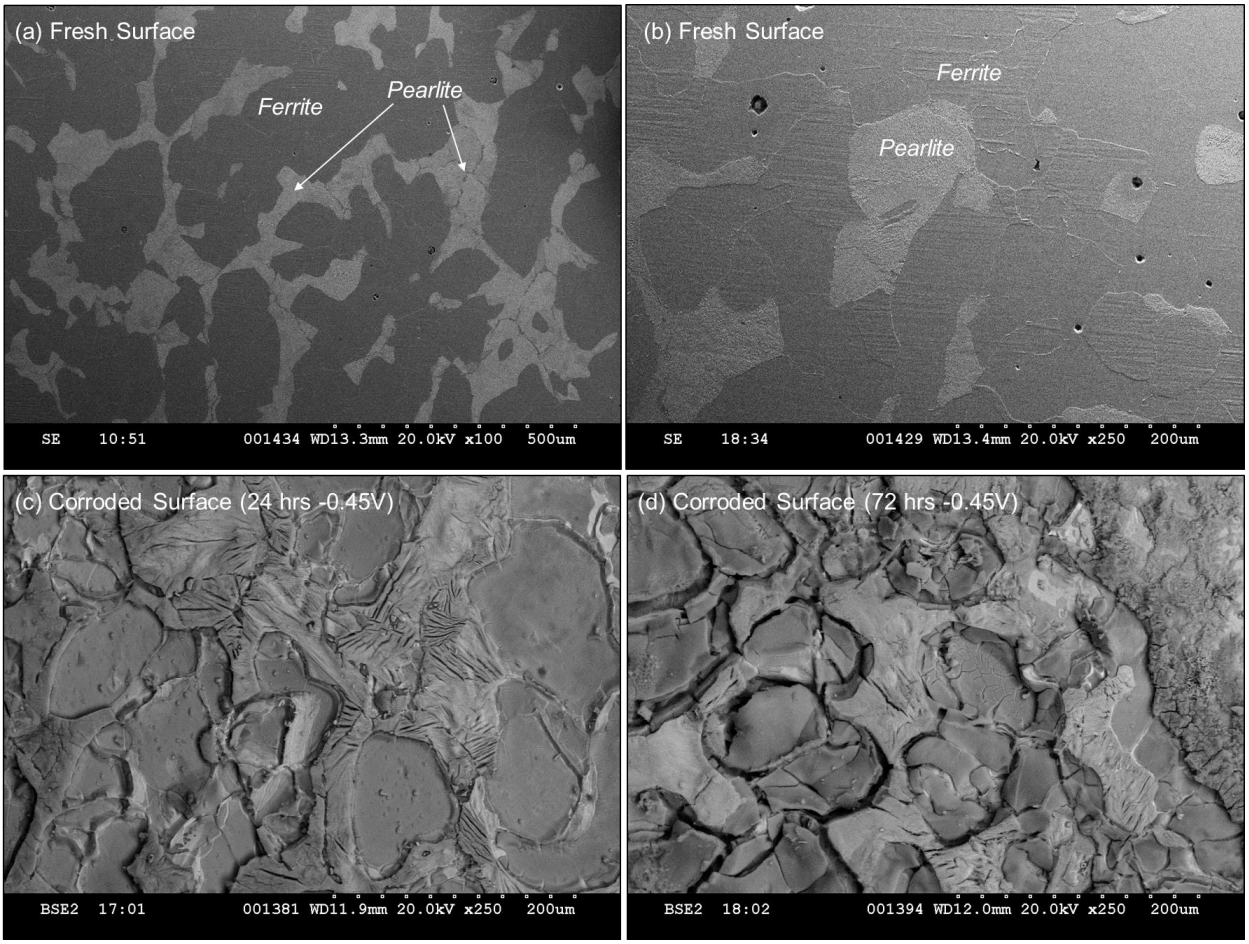

Figure 12. SEM micrographs of the polished unreacted 4320 steel electrodes (a) and (b) and the same electrode after 24 hours (c) and 72 hours (d) under potentiostatic conditions at 0.45 V_{SCE} and pH 4 [Gattu et. al. 2018, NACE].

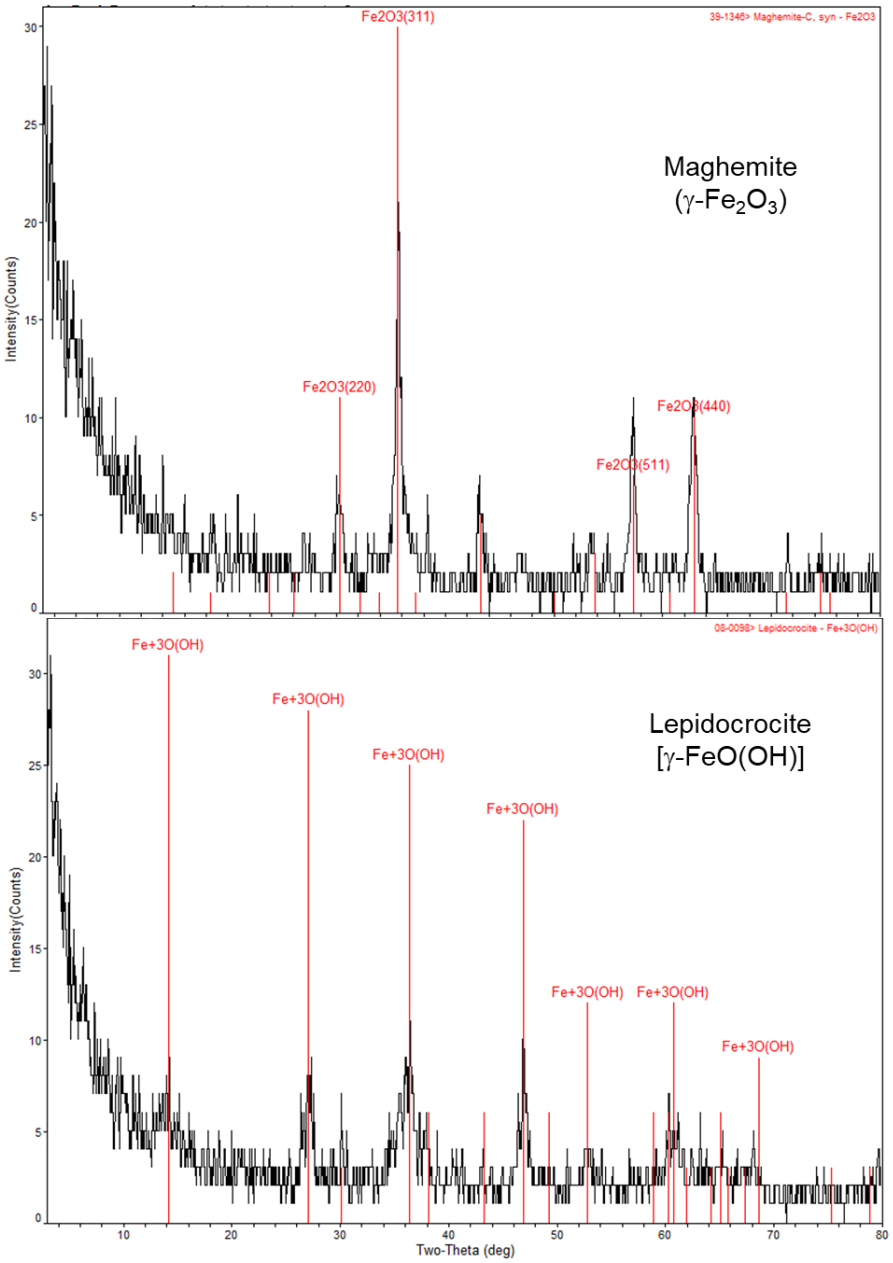

Figure 13. X-ray diffraction scans of oxide corrosion phases from the potentiostatic tests on 4320 carbon steel. The top diagram was for the -0.45 volt hold and the bottom diagram was for the 0.1 volt hold.

The test matrix shown in Table 5 calls for experiments to be performed in both sodium chloride and sodium sulfate solutions of varying concentrations to quantify the effect these anions have on steel and Zircaloy corrosion over a range of repository relevant Eh and pH conditions. The experimental concentrations for chloride and sulfate and other chemical variables such as pH and ionic strength are based on the chemical analyses of the bentonite pore waters presented in Fernandez et al., 2001 (Table 4).

As shown in Table 5, some experiments will be performed in the presence of a UO_2 (or lanthanide doped UO_2) electrode to provide a continuous source of uranium as the UO_2 dissolves at a rate established by the solution chemistry and measured electrochemically. These tests involving the simultaneous corrosion of the alloy and UO_2 will produce samples that can be used to determine if the dissolved uranium is

incorporated into steel corrosion phases. Detailed analytical electron microscopy will be required to both identify the corrosion phases present and to determine their uranium content and disposition. A range of different types of steel corrosion phases can be produced using the electrochemical approach described above as some tests will involve relatively oxidizing potentiostatic holds while others will be held at reducing conditions just above the alloy's corrosion potential in low O_2 environments.

Each electrochemical experiment will generally involve the following sequence of tests:

- potentiodynamic scans to determine E_{corr} of alloy under conditions of interest,
- potentiostatic holds over a range of relevant redox conditions,
- standard electrical impedance spectroscopy to characterize the properties of passivating oxide layers,
- detailed microscopy (reflected light, SEM/EDS) to characterize alloy microstructures before and after corrosion tests.

The results from these tests will provide the following information:

- corrosion rates for stabilized surfaces under controlled environmental conditions,
- electrical properties of the passivated surfaces to provide confidence in their long-term stability,
- analytical expressions for key dependencies (Eh, pH, T, chloride concentration) to formulate rate laws for the corrosion of different materials required to calculate H_2 generation rates in the FMD model.
- corrosion products for further analyses

Table 4. Bentonite pore water chemistry from FEBEX bentonite water extraction tests (adapted from Fernandez et al., 2001).

Measured Values	**Surface:Volume**		
	4.2:1	3.8:1	3.3:1
pH	7.49	7.29	7.38
Species *(mg/L)*			
Cl^-	2200	3600	4000
SO_4^{2-}	603	1100	1260
Br^-	4.9	4.9	9.1
HCO_3^-	67	131	133
SiO_2(aq)	10.9	14.4	N.D.
Al^{3+}	0.34	N.D.	0.12
Ca^{2+}	295	450	510
Mg^{2+}	385	410	390
Na^+	800	1725	2100
K^+	7.5	54	15
Sr^{2+}	6.2	6.9	7.5

N.D.: Not Determined

Table 5. Test matrix for electrochemical experiments. Experiments will determine corrosion rates and mechanisms using standard potentiodynamic polarization, potentiostatic holds and electrical impedance spectroscopy techniques.

Solution Variables	2000 mg/L Cl^- No UO_2			4000 mg/L Cl^- No UO_2			2000 mg/L Cl^- UO_2 Pellet at OC			4000 mg/L Cl^- UO_2 Pellet at OC		
pH	4	7	10	4	7	10	4	7	10	4	7	10
316L SS	FY18	FY18	FY18	FY18	FY18	FY18	FY19	FY19	FY19	FY19	FY19	FY19
304L SS	Future work	Future work	Future work	Future work	Future work	Future work	Future work	Future work	Future work	Future work	Future work	Future work
Carbon Steel (4320)	FY18	FY18	FY18	FY18	FY18	FY18	FY19	FY19	FY19	FY19	FY19	FY19
Borated SS (Neutronit)	Future work	Future work	Future work	Future work	Future work	Future work	Future work	Future work	Future work	Future work	Future work	Future work
Zircaloy-4	FY18	FY18	FY18	FY18	FY18	FY18	NA	NA	NA	NA	NA	NA
Solution Variables	600 mg/L SO_4^{2-} No UO_2			1300 mg/L SO_4^{2-} No UO_2			600 mg/L SO_4^{2-} UO_2 Pellet at OC			1300 mg/L SO_4^{2-} UO_2 Pellet at OC		
pH	4	7	10	4	7	10	4	7	10	4	7	10
316L SS	Future work	Future work	Future work	Future work	Future work	Future work	Future work	Future work	Future work	Future work	Future work	Future work
304L SS	Future work	Future work	Future work	Future work	Future work	Future work	Future work	Future work	Future work	Future work	Future work	Future work
Carbon Steel (4320)	Future work	Future work	Future work	Future work	Future work	Future work	Future work	Future work	Future work	Future work	Future work	Future work
Borated SS (Neutronit)	Future work	Future work	Future work	Future work	Future work	Future work	Future work	Future work	Future work	Future work	Future work	Future work
Zircaloy-4	Future work	Future work	Future work	Future work	Future work	Future work	Future work	Future work	Future work	Future work	Future work	Future work

NA (not applicable) tests with UO2 and Zircaloy will not be performed.
Starting solution composition will from the middle column (3.8:1) shown in Table 1.
All tests to be performed at ambient temperature (will be measured and recorded for each test).
OC: Open Circuit.

4. CONCLUSIONS AND FUTURE WORK

The accomplishments and conclusions of this study are summarized as follows:

- The parameter database for the FMD model was updated based on comparisons between model results and existing spent fuel and UO_2 dissolution rate data.

- Results from sensitivity runs with the new model version (FMDM V.4) reiterate the need for experimental data to parameterize and validate the steel corrosion module added to the FMD model as discussed in Jerden et al., 2017(a) and Jerden et al., 2017(b). Electrochemical tests are in progress to support implementation of an improved steel passivation model in the FMD model by providing data sets with which the model can be calibrated for metals that will be present in the repository engineered barrier system (EBS) and key environmental variables.

- Results from scoping experiments demonstrated a straightforward electrochemical method that provides the electrokinetic information needed for model parameterization and validation.

- Model simulations using the FMDM V.4 agree with previous FMD model results showing that the presence of metals that corrode at different rates can extend the time over which H_2 generation will attenuate the fuel degradation rate. The materials used in the EBS can be selected to benefit the long-term performance of disposed fuel based on their measured corrosion behaviors and impacts on fuel durability as quantified by the FMDM calculations.

Model runs performed for this report demonstrate a number of important information gaps that need to be addressed by experimental work and in further model developments. These information gaps, which were also noted in Jerden et al., 2017(b), are as follows:

- Electrochemical corrosion experiments are needed to quantify the dependencies of spent fuel and steel corrosion rates on environmental variables under carefully controlled conditions. Most importantly, the dependencies of the steel corrosion rates on Eh, pH and the attenuating effect of passivation must be known to calibrate and validate the FMD model. Electrochemically determined corrosion rates are appropriate for calibrating the H_2 generation rates calculated with the FMD steel corrosion module because they quantify the electron transfer rate in the reduction reaction that generates the H_2. Examples of those electrochemical tests are summarized in this report.

- Experimental and modeling studies investigating the corrosion rates of different alloys that may go into the waste package design and waste form degradation are needed. Understanding the corrosion behavior of a variety of relevant engineering materials would provide important insights as to the types of steel that could be used to optimize the long-term performance of the waste package and canister materials. For example, using a combination of actively corroding and passive metals having a range of corrosion rates could be utilized to ensure H_2 would be generated throughout most of the regulated service life. The steel corrosion model developed to quantify H_2 generation from metal surfaces within a breached waste package can also be used to model the corrosion kinetics of external surfaces contacted by bentonite pore water and possibly to model container breaching.

- Electrochemical tests quantifying the kinetic parameters for individual reactions at the in-package solution – spent fuel interface are needed (e.g., see Table 2 above). Based on the use of robust

canisters, it is likely that the majority of the spent fuel in a repository will not be contacted by groundwater until canisters begin to fail more than 1000 years after repository closure. More studies are needed to determine the effects of fuel aging on fuel dissolution rates by measuring dissolution rates of actinide oxide materials that simulate "aged" ~1000 year old fuel in the presence of H_2. Such materials can be represented by doping UO_2 with fission product oxides and actinides. Electrochemical tests to measure the dissolution rates of materials representing aged fuel alone and in the presence of corroding steel will provide the dataset required for reliable model validation to add confidence to the rate predictions.

- Modeling studies that build on our successful model integration efforts are needed. These investigations should focus on the chemical evolution of the in-package solution in contact with degrading spent fuel following the breach of the waste package and Zircaloy cladding. This is particularly important just after a breach due to acid-producing reactions that occur when radiolytic oxidants from the fuel contact reducing groundwaters, as demonstrated in Jerden et al., 2017(b).

5. REFERENCES

Arthur, S., Aqueous Corrosion Rates for Waste Package Materials, ANL-DSD-MD-000001 REV 01, October 2004, DOC.20041012.0003

Bard, A., Faulkner, L., "Electrochemical methods: Fundamentals and Applications", John Wiley and Sons, Inc., 2001

Broczkowski, M.E., Noël, J.J., Shoesmith, D.W., The inhibiting effects of hydrogen on the corrosion of uranium dioxide under nuclear waste disposal conditions, *Journal of Nuclear Materials*, 346, 16–23, 2005

Buck E., Jerden, J., Ebert, W., Wittman, R., "Coupling the Mixed Potential and Radiolysis Models for Used Fuel Degradation," FCRD-UFD-2013-000290, 2013.

Gattu, V.K., Ebert, W.L., Tehrani, N., and Indacochea, J.E. (2018). "Electrochemical Measurements of Steel Corrosion for Modeling H_2 Generation." *Corrosion 2018*, May 11-14, 2018, Phoenix, AZ. Paper No. 11370.

Jerden J. Frey K. Ebert W., "A Multiphase Interfacial Model for the Dissolution of Spent Nuclear Fuel, *Journal of Nuclear Materials*, 462, 135–146, 2015.

Jerden, J., Frey, K., Ebert, W., "Spent Fuel Matrix Degradation and Canister Corrosion: Quantifying the Effect of Hydrogen", Report for Spent Fuel and Waste Science and Technology Project, Report #: SFWD-SFWST-2017-000039, February 28, 2017(a)

Jerden, J., Gattu, V. K., Ebert, W., "Progress Report on Development of the Spent Fuel Degradation and Waste Package Degradation Models and Model Integration", Report for Spent Fuel and Waste Science and Technology Project, Report #: SFWD-SFWST-2017-000091, August 14, 2017(b)

King F. and Kolar M., "An Improved C-Steel Corrosion Model For the Mixed-Potential Model for Used Fuel Dissolution (MPM Version 1.4)," Ontario Hydro, Nuclear Waste Management Division Report No: 06619-REP-01300-l0027-R00, 2001.

King F. and Kolar M., "Validation of the Mixed-Potential Model for Used Fuel Dissolution Against Experimental Data" Ontario Hydro, Nuclear Waste Management Division Report No. 06819-REP-01200-10077-R00, 2002.

King F. and Kolar M., "The Mixed-Potential Model for UO2 Dissolution MPM Versions V1.3 and V1.4," Ontario Hydro, Nuclear Waste Management Division Report No. 06819-REP-01200-10104 R00, 2003.

King, F., "Overview of a Carbon Steel Container Corrosion Model for a Deep Geological Repository in Sedimentary Rock," Nuclear Waste Management Organization Report TR-2007-01, March 2007, 71 p.

Ollila, K., "Dissolution of Unirradiated UO_2 and UO_2 Doped with ^{233}U in Low- and High-Ionic-Strength NaCl Under Anoxic and Reducing Conditions," Posiva Working Report 2008-50, 2008.

Radulescu, G., "Repository Science/Criticality Analysis," Oak Ridge National Laboratory, Reactor and Nuclear Systems Division Report: FTOR11UF0334, ORNL/LTR-2011, Oak Ridge National Laboratory, Oak Ridge, TN., 2011.

Röllin S., Spahiu K., Eklunda U., "Determination of Dissolution Rates of Spent Fuel in Carbonate Solutions Under Different Redox Conditions with a Flow-through Experiment," *Journal of Nuclear Materials*, vol. 297, pp. 231–243, 2001.

Shoesmith, D.W. and F. King. 1998. A mixed-potential model for the prediction of the effects of α-radiolysis, precipitation and redox processes on the dissolution of used nuclear fuel. Ontario Hydro, Nuclear Waste Management Division Report 06819-REP-01200-0038- R00. Toronto, Ontario.

Shoesmith, D., "The Role of Dissolved Hydrogen on the Corrosion/Dissolution of Spent Nuclear Fuel," Nuclear Waste Management Organization, Toronto, Ontario, Canada, TR-2008-19, November 2008.

Wang Y. et al., "Used Fuel Disposal in Crystalline Rocks: Status and FY14 Progress," FCRD-UFD-2014-000060, SAND2014, Sandia National Laboratories, Albuquerque, NM., 2014.